

Phase 1 Study of the Pittsburgh Compound B Derivative ^{18}F -Flutemetamol in Healthy Volunteers and Patients with Probable Alzheimer Disease

Natalie Nelissen^{*1}, Koen Van Laere^{*2}, Lennart Thurfjell³, Rikard Owenius³, Mathieu Vandenberghe⁴, Michel Koole², Guy Bormans⁵, David J. Brooks^{6,7}, and Rik Vandenberghe^{1,8}

¹Laboratory for Cognitive Neurology, K.U. Leuven, Leuven, Belgium; ²Division of Nuclear Medicine, University Hospitals Leuven, Leuven, Belgium; ³GE Healthcare, Medical Diagnostics, Research and Development, Uppsala, Sweden; ⁴Division of Psychiatry, University Hospitals Leuven, Leuven, Belgium; ⁵Laboratory for Radiopharmacy, K.U. Leuven, Leuven, Belgium; ⁶GE Healthcare, Medical Diagnostics, Research and Development, London, United Kingdom; ⁷Division of Neuroscience, Faculty of Medicine, Imperial College London, London, United Kingdom; and ⁸Neurology Department, University Hospitals Leuven, Leuven, Belgium

^{11}C -Pittsburgh compound B (PiB) marks A β amyloidosis, a key pathogenetic process in Alzheimer disease (AD). The use of ^{11}C -PiB is limited to centers with a cyclotron. Development of the ^{18}F -labeled thioflavin derivative of PiB, ^{18}F -flutemetamol, could hugely increase the availability of this new technology. The aims of this phase 1 study were to perform brain kinetic modeling of ^{18}F -flutemetamol, optimize the image acquisition procedure, and compare methods of analysis (step 1) and to compare ^{18}F -flutemetamol brain retention in AD patients versus healthy controls in a proof-of-concept study (steps 1 and 2). **Methods:** In step 1, 3 AD patients (Mini-Mental State Examination, 22–24) and 3 elderly healthy controls were scanned dynamically during windows of 0–90, 150–180, and 220–250 min after injection of approximately 180 MBq of ^{18}F -flutemetamol, with arterial sampling. We compared different analysis methods (compartmental modeling, Logan graphical analysis, and standardized uptake value ratios) and determined the optimal acquisition window for step 2. In step 2, 5 AD patients (Mini-Mental State Examination, 20–26) and 5 elderly healthy controls were scanned from 80 to 170 min after injection. To determine overall efficacy, steps 1 and 2 were pooled and standardized uptake value ratios were calculated using cerebellar cortex as a reference region. **Results:** No adverse events were reported. There was a strong correlation between uptake values obtained with the different analysis methods. From 80 min after injection onward, the ratio of neocortical to cerebellar uptake was maximal and only marginally affected by scan start time or duration. AD patients showed significantly increased standardized uptake value ratios in neocortical association zones and striatum, compared with healthy controls, whereas uptake in white matter, cerebellum, and pons did not differ between groups. Two AD patients were

^{18}F -flutemetamol-negative and 1 healthy control was ^{18}F -flutemetamol-positive. **Conclusion:** ^{18}F -flutemetamol uptake can be readily quantified. This phase 1 study warrants further studies to validate this ^{18}F -labeled derivative of PiB as a biomarker for A β amyloidosis.

Key Words: A β amyloid; ^{18}F -flutemetamol; PET; Alzheimer's disease

J Nucl Med 2009; 50:1251–1259

DOI: 10.2967/jnumed.109.063305

Alzheimer disease (AD) is neuropathologically characterized by synapse loss, neuritic A β amyloid plaques, and neurofibrillary tangles. Making an accurate and reliable diagnosis of AD at the earliest disease stages is challenging and becomes increasingly important as disease-modifying therapies, such as those aimed at lowering A β amyloid, appear on the horizon.

In 2004, Klunk et al. presented a novel method for the in vivo detection of A β amyloid plaques in the brain using the thioflavin-T analog PET tracer ^{11}C -Pittsburgh compound B (PiB) (*1*). In vitro binding of this ligand to brain homogenates correlates tightly with total insoluble A β and A β_{1-42} levels (*2,3*). In vivo ^{11}C -PiB uptake in AD or Lewy body disease correlates with the topography and intensity of A β amyloid aggregates measured neuropathologically in the same brains (*4–7*). ^{11}C -PiB PET marks not only parenchymal A β but also A β deposits in vessel walls (*4,8–11*). At the low or subnanomolar administered concentrations of PET ligands in vivo, PiB does not bind to neurofibrillary tangles (*2,10*) or α -synuclein fibrils (*12*).

Having a good ^{18}F A β tracer would increase the availability of this new technology by more than 10-fold (*13*). ^{18}F -flutemetamol (previously known as ^{18}F -GE067) (*14*) is

Received Feb. 13, 2009; revision accepted Apr. 28, 2009.

For correspondence or reprints contact: Rik Vandenberghe, Laboratory for Cognitive Neurology, UZ Leuven, Herestraat 49–bus 7003, 3000 Leuven, Belgium.

E-mail: rik.vandenberghe@uz.kuleuven.be

*Contributed equally to this work.

COPYRIGHT © 2009 by the Society of Nuclear Medicine, Inc.

a PiB derivative radiolabeled with ^{18}F . Extensive validation of the PiB parent molecule is an important advantage on the way toward validation of ^{18}F -flutemetamol (13). Other ^{18}F -labeled amyloid imaging agents for clinical use in humans include the naphthol 2-(1-{6-[(2- ^{18}F]fluoroethyl)(methyl)-amino]-2-naphthyl}ethylidene)malononitrile (^{18}F -FDDNP), which labels both A β amyloid plaques and neurofibrillary tangles (15,16), and, more recently, the stilbenes ^{18}F -BAY94-9172 (^{18}F -AV1) and ^{18}F -AV45 (17).

The biodistribution and internal radiation dosimetry of an intravenous injection of ^{18}F -flutemetamol have been reported before (14). The primary aims of the current phase 1 study were to perform brain kinetic modeling of ^{18}F -flutemetamol, select the optimal image acquisition window, and compare different methods of analysis (step 1) and to contrast ^{18}F -flutemetamol brain retention in AD patients versus healthy controls in a proof-of-concept study (steps 1 and 2).

MATERIALS AND METHODS

Subjects

Eight patients with early-stage clinically probable AD were recruited via the academic memory clinic of the University Hospitals Leuven. Three participated in step 1, and 5 in step 2. Subjects had to fulfill the criteria of the National Institute of Neurological and Communicative Disorders and Stroke and of the Alzheimer's Disease and Related Disorders Association for clinically probable AD (18) and the DSM-IV criteria for dementia of Alzheimer type (19). Mini-Mental State Examination scores had to lie between 18 and 26 of 30, and the Clinical Dementia Rating (20) between 0.5 and 2, with a score lower than 4 on the Modified Hachinski Ischemic scale. Patient demographics and neuropsychologic test results are listed in Table 1. All patients were

receiving stable treatment with a cholinesterase inhibitor, 5 were taking a selective serotonin-reuptake inhibitor, and 1 was receiving quetiapine, 100 mg once a day.

Eight healthy controls, 5 men and 3 women, were recruited through an advertisement in a local newspaper asking for volunteers to participate in a scientific study with brain imaging. Three participated in step 1, and 5 in step 2. The subjects had to be older than 50 y, with a Mini-Mental State Examination score above 27 and a Clinical Dementia Rating of 0. Abnormalities on detailed neuropsychologic testing and 2 or more first-degree relatives with a diagnosis of AD were among the exclusion criteria for participation as a healthy control.

All participants gave written informed consent in accordance with the Declaration of Helsinki. The protocol was approved by the Ethical Committee of the University Hospitals Leuven.

Radiochemical Production of ^{18}F -Flutemetamol

The investigational medicinal product ^{18}F -flutemetamol (Fig. 1A) (containing the drug substance AH110690) was batch-manufactured according to good manufacturing guidelines (EudraLex, volume 4, annex 3) at the Cyclotron Research Centre, University of Liège, using a TracerLab-FX_{F-N} chemistry platform (GE Healthcare). The chemical and radiochemical purity of the test item were assessed by an analytic high-performance liquid chromatograph equipped with an ultraviolet and radioactivity detector. The total AH110690 chemical content was 0.7 ± 0.3 $\mu\text{g/mL}$, and the radiochemical purity was $98.1\% \pm 1.2\%$. The identity of the radiolabeled product was confirmed by coelution on high-performance liquid chromatography of a cold analytic standard of AH110690.

^{18}F -flutemetamol was supplied as a ready-to-inject solution with an upper limit fixed at 10 μg of cold AH110690 per dose, in line with good manufacturing guidelines, and the solution for

TABLE 1. Demographics and Neuropsychologic Results

Demographic	AD patient no.								Mean controls	SD controls
	1	2	3	4	5	6	7	8		
Sex	M	M	M	M	F	M	M	F		
Age (y)	63	55	68	77	73	73	68	72	62.5	7.1
MMSE (/30)	24*	23*	22*	22*	20*	26*	23*	25*	28.9	0.99
Clinical dementia rating	0.5	0.5	0.5	0.5	1	0.5	0.5	0.5	0	0
Digit span										
Forward	6	3*	5	6	5	4	4	5	6.6	1.8
Backward	6	2*	2*	6	4	5	3	6	6.6	1.8
ADAS, cognitive										
List learning (/10)	7*	6*	6*	7*	9*	6*	6*	6*	3.0	0.9
Delayed recall (/10)	10*	10*	10*	10*	10*	10*	10*	10*	3.0	1.3
Recognition (/12)	2	3	5	3	11*	4	2	3	1.6	2.3
Animal verbal fluency	15	8*	9*	12	6*	10*	11	9*	19.8	4.6
Letter verbal fluency	40	21	31	16	19	29	22	25	27.9	7.0
Boston naming test (/60)	56	51	39*	50	33*	48	38*	43*	54.0	5.3
TMT B/A	2.2	3.3	2.7	5.7*	—	3.0	4.0*	6.5*	2.7	0.7
Stroop interference	43.6	50.6	24.2	50.4	—	−9.2	7.2	18.2	11.6	24.6

*More than 2 SDs below average score of healthy controls.

MMSE = Mini-Mental State Examination; ADAS, cognitive = Alzheimer disease assessment scale, cognitive subscale; list learning = missed items averaged over 3 learning trials; delayed recall = missed items; recognition = sum of false-positive and false-negative responses (if sum exceeds 12, score is 12); TMT B/A = trail-making test; Stroop interference = time spent on interference card minus (time on color card \times 1.8–11).

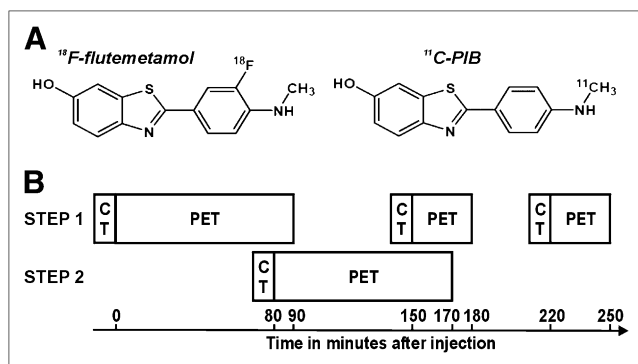


FIGURE 1. (A) Chemical structure of ^{18}F -flutemetamol and ^{11}C -PiB parent molecule. (B) Acquisition scheme in steps 1 and 2.

injection contained 7% ethanol (v/v) and 0.5% polysorbate 80 (w/v) in phosphate buffer (0.015 M).

PET Acquisition

^{18}F -flutemetamol was injected intravenously as a slow bolus in an antecubital vein (AD patients: 180.9 ± 5.4 MBq (mean \pm SD), with a range of 171.5–187.6 MBq; healthy controls: 179.6 ± 3.8 MBq, with a range of 172.5–184.7 MBq). Dynamic brain scanning was performed using a 16-slice Biograph PET/CT scanner (Siemens) in 3-dimensional list mode.

In step 1 of the study, PET data acquisition was started at the time of tracer injection and lasted for 90 min; a second period of data acquisition ran from 150 to 180 min, and a third ran from 220 to 250 min. Before the start of each PET epoch, subjects were repositioned in the scanner and a low-dose CT scan was obtained (Fig. 1B).

In step 2, the acquisition procedure was simplified on the basis of time–activity curves obtained in step 1: data acquisition was limited to 80–170 min after injection, with the option of aborting the scan at 140 min, which was requested by 2 healthy controls. A low-dose CT scan was acquired before the PET scan (Fig. 1B).

PET data were corrected for attenuation (based on the CT scan), randoms, and scatter using the manufacturer's software. Data were reconstructed using Fourier rebinning and 2-dimensional ordered-subsets expectation maximization (81 axial slices, 5 iterations and 8 subsets, 128×128 matrix, $2.5\times$ zoom, 2.13-mm pixels, 2-mm slice thickness, 2-mm slice separation, gaussian postsmoothing with a full width at half maximum of 5 mm, and no smoothing in the axial direction). Full dynamic data acquired in step 1 were reconstructed as 4×30 , 6×60 , 4×180 , 8×300 , 3×600 , 3×600 , and 3×600 s time frames. Step 2 data were reconstructed as 18×300 s frames.

MRI Acquisition

MRI scans were acquired with an Intera 1.5-T scanner (Philips) within 30 d before the subject's PET scan. The scanning protocol included a high-resolution structural T1-weighted image (3-dimensional magnetization-prepared rapid gradient echo, 10-s repetition time, 4-ms echo time, 20-ms inversion time, 500-ms delay time, 10° flip angle, 256×256 matrix, and 1-mm^3 voxels) and a fluid attenuation inversion recovery scan (coronal 5-mm slices, 5-s repetition time, 110-ms echo time, 1,850-ms inversion time, 256×256 matrix, 200-mm field of view, and 2 acquisitions). For

technical reasons, the T1-weighted image was not available for 2 subjects.

Discrete Blood Sampling and Parent Analysis

In step 1, arterial blood samples (3 mL) were collected at 10-s intervals during the first minute, at 15-s intervals during minutes 2 and 3, and at 4, 8, 15, 30, 45, 60, 90, 120, 180, and 240 min after injection. Red blood cells were removed by centrifugation. The counts/s were measured with a well counter and translated into activity concentration data in Bq/mL, decay-corrected to the time of tracer administration.

In addition, arterial blood samples (2 mL) were collected at 2, 5, 20, 60, and 180 min after injection to determine the percentage of radioactive parent compound and metabolites. Blood samples were centrifuged, and the separated plasma supernatant was collected. The plasma was mixed with a solution of reference flutemetamol in acetonitrile and then injected onto the high-performance liquid chromatography system (LaChrom Elite; Hitachi) equipped with a Chromolith Performance RP-18e (100×3 mm) column (Merck). Separation was performed with a gradient elution protocol. With guidance by the ultraviolet signal, 3 fractions were collected (before, during, and after the ^{18}F -flutemetamol peak), and the radioactivity was measured in the γ -sample changer.

Image Preprocessing

The 3 dynamic PET scans of step 1 were concatenated. For steps 1 and 2, the voxel values of all frames were decay-corrected to the time of ^{18}F -flutemetamol administration. All PET frames were realigned using an automated method (21), and a PET sum image was created. The MRI scan was coregistered to the PET summed image using a mutual information–based method (22). The MRI scans were spatially normalized into Montreal Neurologic Institute space using a second-order polynomial transformation and normalized mutual information as the cost function (23). The normalization matrix was then applied to the coregistered PET scans.

Volume-of-Interest (VOI) Analysis

Twelve VOIs were drawn on an MRI template in Montreal Neurologic Institute space. VOIs included the lateral frontal cortex, medial temporal cortex, lateral temporal cortex, lateral parietal cortex, occipital cortex, striatum, sensorimotor cortex, anterior cingulate, posterior cingulate, pons, subcortical white matter, and cerebellar cortex. In addition, a composite cortical VOI was defined by taking the volume-weighted average of lateral frontal, lateral temporal, lateral parietal, anterior, and posterior cingulate regions. For each subject, the VOIs were checked against the subject's spatially normalized MR image, and adjustments were made if necessary. Time–activity curves were generated from bilateral homologous VOIs. As in previous A β amyloid-imaging PET studies (1,17,24), the cerebellar cortex was selected as the primary reference region because it is notably free of fibrillary plaques. Because A β amyloid plaques are absent in the pons (25), and ^{11}C -PiB uptake in this area is similar in AD patients and controls (1), we also evaluated whether similar results could be obtained with the current compound if the pons was used as a reference region.

Compartmental Modeling of Step 1 Data

A 2-tissue-compartment model, arterial input function (2TC-4k) (26), was applied to the step 1 data to characterize the influx (K_1 , $\text{mL}\cdot\text{cm}^{-3}\cdot\text{min}^{-1}$) and efflux (k_2 , min^{-1}) across the blood–

brain barrier (first compartment), and binding (k_3 , min^{-1}) and release (k_4 , min^{-1}) (second compartment) of ^{18}F -flutemetamol within the defined VOIs. The general assumption was that free and nonspecific tracer compartments were indistinguishable. Constant cerebral blood volumes were assumed (0.02 in pons and subcortical white matter, 0.035 in striatum, 0.05 in cerebellar and occipital cortex, and 0.04 in the remaining cortical regions (27)). Using the arterial input function (corrected for the presence of metabolites) and regional time–activity curves as model inputs, we established the kinetic rate constants by iterative curve fitting. The most important parameters derived from the 2TC-4k model, reflecting specific tracer binding, were the total distribution volume, V_T , which equals $K_1/k_2(1 + k_3/k_4)$, and the distribution volume ratio, DVR, which is a normalization of the regional V_T by the nonspecific retention in the reference region. For comparison, the special cases in which $k_4 = 0$ or $k_3 = k_4 = 0$ were also studied. The performance of different model configurations was assessed using the Akaike information criterion (AIC) expressed as percentages, that is, how much lower (better) a model's AIC was than the AIC of the comparison model.

Graphical Analysis of Step 1 Data

An alternative quantification approach is the Logan graphical analysis method (28), which is appropriate for reversible in vivo kinetics. This method linearizes the kinetics of brain uptake of the tracer in tissue after it has equilibrated with the tracer in plasma. Logan analysis was applied over the 60- (or 70-) to 250-min PET scan interval of the step 1 data. Constant cerebral blood volumes were assumed (as above), and the equation of the linear function was estimated by least-squares linear regression.

The slope of the linearization is equivalent to either the tracer V_T or the DVR, depending on whether the input function is the arterial input function (“input-Logan” approach) or the time–activity curve of a reference region acting as an indirect input function (“reference-Logan” approach), respectively.

Standardized Uptake Value (SUV) Ratio Analysis of Pooled Step 1 and Step 2 Data

The SUV ratio is a semiquantitative measure of tracer uptake, normalized for the mean uptake in a reference region, and does not require arterial blood sampling or dynamic imaging. SUV ratio is defined as the ratio of SUV in the VOI to SUV in a reference region, with SUV being the integrated activity over a given period per unit of injected dose and body weight.

To maximize the data available for analysis, a common time epoch (85–170 min) was interrogated from the combined step 1 and step 2 data. Because step 1 data were acquired from 0 to 90, 150 to 180, and 220 to 250 min after injection, an exponential function was fitted to the time–activity curves and used to interpolate regional brain uptake over the 90- to 150-min interval.

We also evaluated the impact of scanning start time after injection and scanning length on discrimination between the healthy control and AD groups: for each combination of start times (85–165 min) and window lengths (5–40 min), SUV ratios were calculated for each VOI and subject, and the discrimination between the groups was analyzed. For start times toward the end of the interval, the maximum window length was constrained to never overflow the end of the interval (170 min).

Statistical Analysis

Least-squares linear regression was used to evaluate the relationships between DVR and SUV ratios in the step 1 data, and the

strength of the correlation was assessed by means of the coefficient of determination (r^2). A 1-sided Wilcoxon/Mann–Whitney nonparametric test was used to assess whether AD scans showed higher uptake in the VOIs relative to the control scans (steps 1 and 2 combined). Statistical tests used a 0.05 significance level, and analyses were performed using the software “R,” version 2.8.0 (<http://www.R-project.org>).

Voxel-Based Analysis

Voxel-based analysis was used to determine the topography of tracer binding in an unbiased manner. SUV ratio images were calculated by summing normalized PET data over 80–90 min and dividing every voxel value by the mean value in the cerebellar cortex. Before statistical analysis, SUV ratio images were smoothed with an isotropic gaussian kernel of 12 mm in full width at half maximum. Voxelwise 2-sample t tests (SPM2, Statistical Parametric Mapping, Wellcome Department of Cognitive Neurology) were used to determine differences between AD patients and the control group, thresholded at a voxel-level $P < 0.05$ corrected for the whole brain volume.

RESULTS

Step 1: Optimization of Acquisition and Comparison of Analysis Procedures

Plots of the ^{18}F -flutemetamol arterial plasma activity concentration as a function of time were similar across groups, and a reasonable representation of the bolus peak was obtained for all step 1 subjects. The parent analysis showed polar metabolites and similar metabolism in AD patients and healthy controls. The amount of intact ^{18}F -flutemetamol decreased rapidly over time and was $84.7\% \pm 4.8\%$ (control) and $77.5\% \pm 2.7\%$ (AD) after 2 min, $23.8\% \pm 1.0\%$ (control) and $27.0\% \pm 2.4\%$ (AD) after 20 min, and $12.2\% \pm 1.9\%$ (control) and $15.3\% \pm 3.4\%$ (AD) after 60 min. After about 180 min, the amount was $7.3\% \pm 1.9\%$ (control) and $13.4\% \pm 0.6\%$ (AD), but counting statistics were poor. The arterial input function was obtained by correcting the arterial plasma activity for the amount of intact ^{18}F -flutemetamol.

Time–activity curves (Fig. 2) indicated that at 80 min after injection the ratio of cortical versus cerebellar SUV was maximal in AD patients and healthy controls and remained approximately constant over the following 90 min.

Compartmental Modeling of Step 1 Data

The cortical and striatal regional time–activity curves were well described by the 2TC-4k compartment model. Setting k_4 to 0 (assuming irreversible tracer binding) clearly did not fit the data as well ($\text{AIC} = 16\% \pm 4\%$ when all cortical regions and subjects were considered), indicating that the specific binding of ^{18}F -flutemetamol to these tissues was reversible. In cerebellum, the 2TC-4k modeling of the time–activity curve showed only a marginal improvement in quality of fit over the simpler 1-tissue-compartment model (1TC-2k) modeling result in 3 subjects ($\text{AIC} = 3.1\% \pm 3.7\%$). For the remaining 3 subjects, the 2TC-4k modeling result was better ($\text{AIC} = 11\% \pm 2\%$) and the $k_3/k_4 > 0$ component was assigned as nonspecific retention since uptake levels in

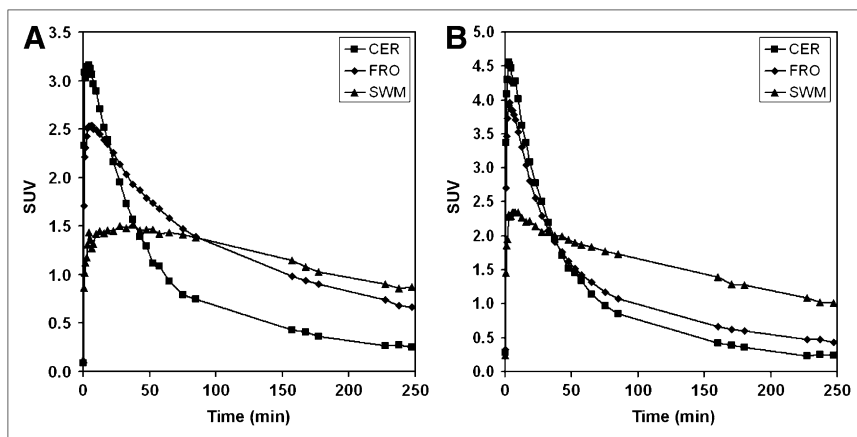


FIGURE 2. Representative examples of time-activity curves for cerebellum (CER), frontal cortex (FRO), and subcortical white matter (SWM) in AD patient 2 (A) and healthy control 2 (B). SUV is activity concentration in VOI/(injected dose/subject weight).

cerebellum were similar in controls and AD patients and specific binding was negligible. The same assignment could be made for the second compartment (k_3 , k_4) for pons and subcortical white matter.

Graphical Analysis of Step 1 Data

Table 2 lists DVR values obtained by the 2TC-4k model and by the input-Logan and reference-Logan approaches, using cerebellum as the reference region. Logan graphical analysis produced adequate linearization over the studied time window for all regions across subjects.

The correlation between DVRs obtained with 2TC-4k and input-Logan (Fig. 3A), as well as with input-Logan and reference-Logan (Fig. 3B), was determined for all VOIs

across all 6 subjects. The 3 methods were highly correlated overall, with a regression slope of 0.88 (2TC-4k vs. input-Logan) and 1.01 (input-Logan vs. reference-Logan) for all regions and subjects taken together.

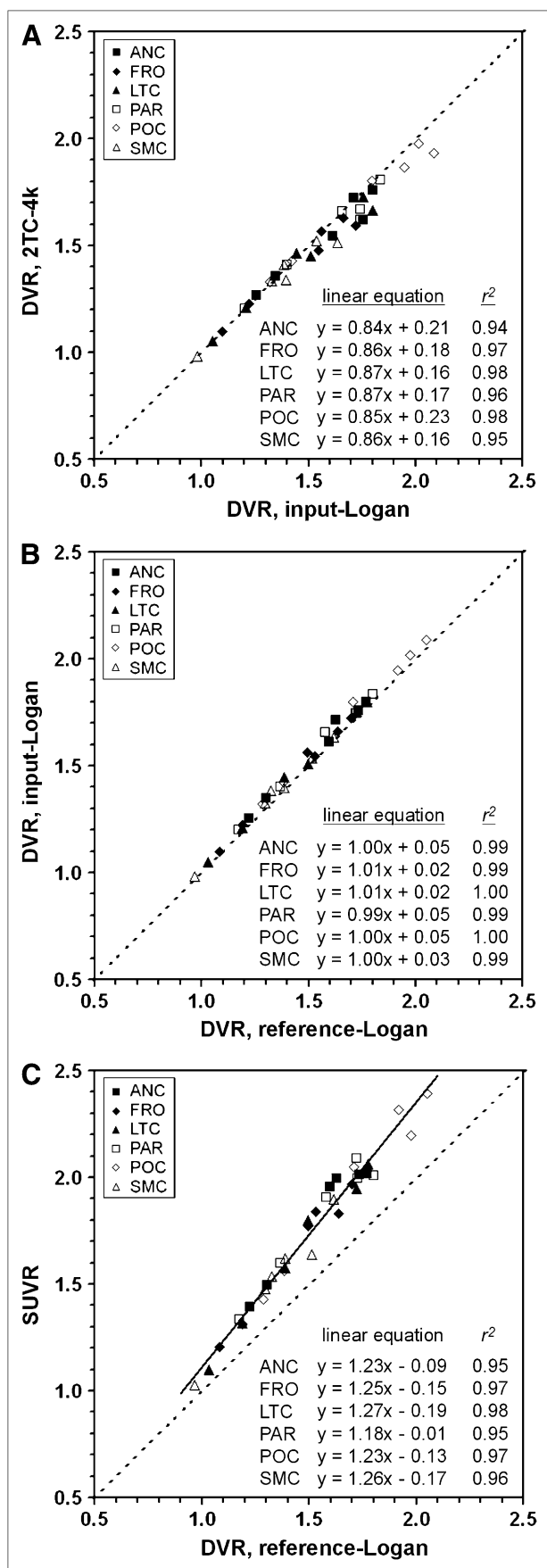
SUV Ratio Analysis of Step 1 Data

There was a tight linear relation between SUV ratio (scan window, 85–105 min) and DVR values from the reference-Logan analysis for all VOIs, with SUV ratio being slightly higher and more responsive than DVR to an increasing ^{18}F -flutemetamol concentration in cortical regions (Fig. 3C).

A similar linear relation was found between SUV ratio and DVR from a reference-Logan analysis when the pons was used as the reference region (slope = 1.15, $r^2 = 0.99$),

TABLE 2. Regional DVRs of ^{18}F -Flutemetamol in AD Patients and Healthy Controls Using 3 Modeling Approaches

	Regional DVR											V _T (CER)
Subject	ANC	FRO	LTC	MTC	OCC	PAR	POC	SMC	STR	PON	SWM	
2T-4k												
HC 1	1.72	1.57	1.46	1.19	1.47	1.66	1.80	1.41	1.59	2.03	2.35	4.40
HC 2	1.36	1.23	1.05	1.04	1.10	1.21	1.33	0.98	1.44	2.02	2.11	5.60
HC 3	1.27	1.10	1.21	1.14	1.50	1.41	1.43	1.34	1.51	2.19	2.42	4.29
AD 1	1.76	1.63	1.73	1.24	1.18	1.81	1.98	1.52	1.80	2.08	2.18	4.45
AD 2	1.62	1.59	1.67	1.09	1.28	1.62	1.94	1.51	1.67	1.66	1.68	3.49
AD 3	1.55	1.48	1.45	1.10	1.26	1.67	1.87	1.34	1.67	1.75	1.93	3.47
Input-Logan												
HC 1	1.71	1.56	1.45	1.19	1.43	1.66	1.80	1.39	1.60	2.00	2.30	4.40
HC 2	1.35	1.22	1.05	1.04	1.09	1.20	1.32	0.98	1.44	2.01	2.08	5.62
HC 3	1.26	1.10	1.21	1.15	1.49	1.40	1.42	1.33	1.50	2.18	2.36	4.31
AD 1	1.80	1.66	1.75	1.27	1.20	1.83	2.02	1.54	1.86	2.15	2.19	4.35
AD 2	1.76	1.72	1.80	1.19	1.38	1.74	2.09	1.63	1.80	1.78	1.80	3.22
AD 3	1.61	1.55	1.51	1.15	1.31	1.74	1.95	1.40	1.74	1.83	1.98	3.34
Reference-Logan												
HC 1	1.63	1.49	1.39	1.16	1.37	1.58	1.71	1.32	1.55	1.93	2.12	—
HC 2	1.30	1.19	1.03	1.02	1.06	1.17	1.28	0.97	1.42	1.99	1.94	—
HC 3	1.22	1.08	1.19	1.14	1.44	1.37	1.38	1.30	1.48	2.14	2.19	—
AD 1	1.77	1.64	1.72	1.26	1.19	1.80	1.98	1.51	1.84	2.14	2.15	—
AD 2	1.73	1.70	1.78	1.19	1.38	1.72	2.05	1.62	1.77	1.75	1.79	—
AD 3	1.60	1.53	1.50	1.15	1.31	1.72	1.92	1.39	1.72	1.82	1.96	—
ANC = anterior cingulate; FRO = frontal cortex; LTC = lateral temporal cortex; MTC = medial temporal cortex; OCC = occipital cortex; PAR = parietal cortex; POC = posterior cingulate; SMC = sensorimotor cortex; STR = striatum; PON = pons; SWM = subcortical white matter; CER = cerebellum; HC = healthy control.												



but here SUV ratios were slightly lower ($8.5\% \pm 6.2\%$) than DVR (data not shown).

The comparison of step 1 results for the various analysis methods clearly revealed similar trends and discrimination capabilities between AD patients and healthy control subjects, despite the different models (compartmental and Logan DVRs) and inputs (arterial and reference region). This finding both motivated and justified the use of the simple SUV ratio method in the pooled analysis to compare AD patients and healthy controls. On the basis of the time-activity curves obtained in step 1 (Fig. 2), we selected 80 min as the starting time of the acquisition for step 2.

SUV Ratio Group Comparison of AD Patients Versus Healthy Controls (Steps 1 and 2 Pooled)

For the pooled step 1 and step 2 data, the SUV ratio analysis found good discrimination between healthy controls and AD patients (Fig. 4). Nearly all cortical brain areas (Fig. 5A) showed a significant difference in SUV ratio (85- to 105-min window) between AD patients and healthy controls, except medial temporal cortex ($P = 0.36$) and occipital cortex ($P = 0.22$). Striatal SUV ratio analysis also showed significant discrimination between the AD and control groups ($P = 0.005$). SUV ratio in pons ($P = 0.90$) and subcortical white matter ($P = 0.75$) did not differ between groups.

In AD patients 6 and 7, SUV ratios in the cortical VOIs overlapped with the SUV ratio range seen in healthy controls (Fig. 5). Conversely, healthy control 1 demonstrated in the cortical VOIs high SUV ratios that were at the lower end of the SUV ratio range seen in subjects with probable AD.

Figure 5B compares the discriminating ability of SUV ratios (85–105 min) for the composite cortical VOI using either cerebellum or pons as the reference region. The discrimination between the 8 AD patients and 8 healthy controls was found to be more significant when cerebellum was used as the reference region ($P = 0.007$) than when pons was used ($P = 0.019$). The subject rank order also differed for the 2 parameters (Fig. 5B).

Analysis of SUV ratio versus start time showed a slight increase with later scanning times in the 85- to 170-min window (Fig. 6A), especially for the cortical regions with elevated uptake in AD patients, but the rank order was nearly constant. Later scan start times resulted in only a minor improvement in discrimination between AD patients and

FIGURE 3. Data for step 1. Correlation plots for cortical regions showing highest ^{18}F -flutemetamol uptake in AD patients: DVR from 2TC-4k model vs. DVR from input-Logan approach (A), DVR from input-Logan approach vs. DVR from reference-Logan approach (B), and SUVR averaged over 85–105 min vs. DVR from reference-Logan approach (C). r^2 = coefficient of determination. ANC = anterior cingulate; FRO = frontal cortex; LTC = lateral temporal cortex; PAR = parietal cortex; POC = posterior cingulate; SMC = sensorimotor cortex; SUVR = SUV ratio.

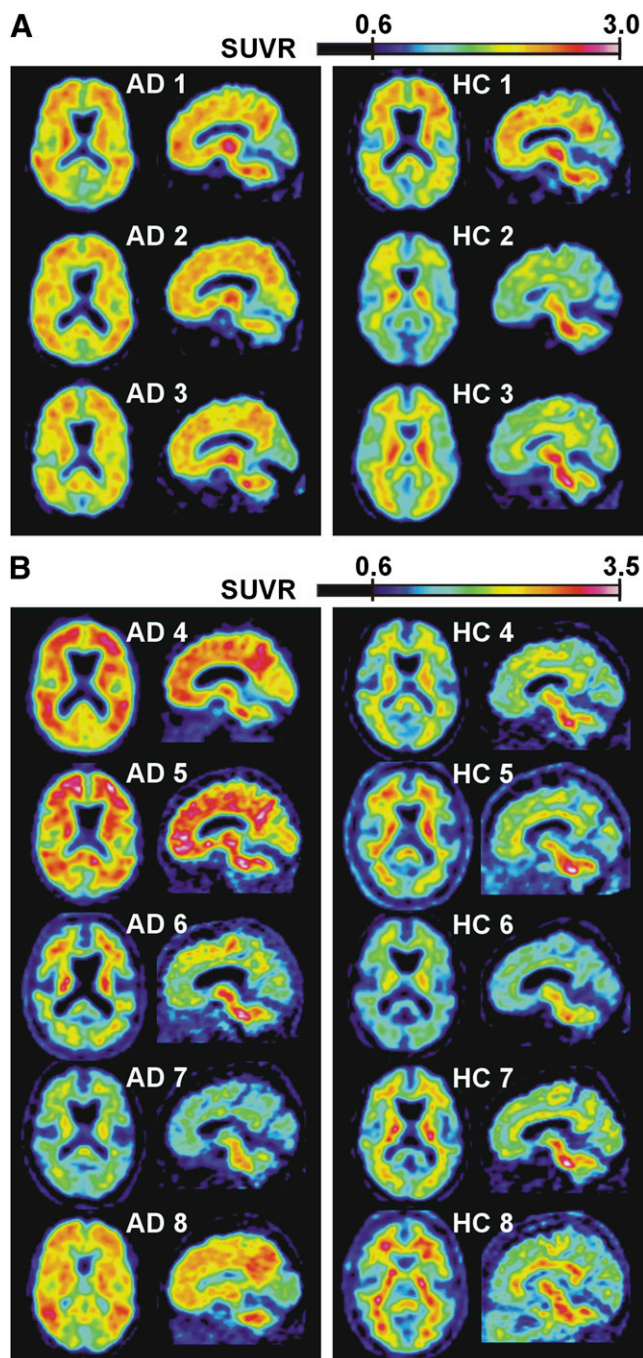


FIGURE 4. Axial and sagittal SUV ratio images in step 1 (70–90 min) (A) and step 2 (85–105 min) (B) in AD patients and healthy controls. Cerebellar cortex was used as reference region. SUV ratio upper limit was set at higher value in B than in A to compensate for increasing SUV ratio at later scan times (Fig. 6). SUV = SUV ratio.

healthy controls. Discrimination between patients and controls was only marginally affected by different scanning lengths (5–40 min), and scanning times as short as 5–10 min were adequate (Fig. 6B).

To elucidate the topography of ^{18}F -flutemetamol uptake, we compared the six ^{18}F -flutemetamol-positive AD patients

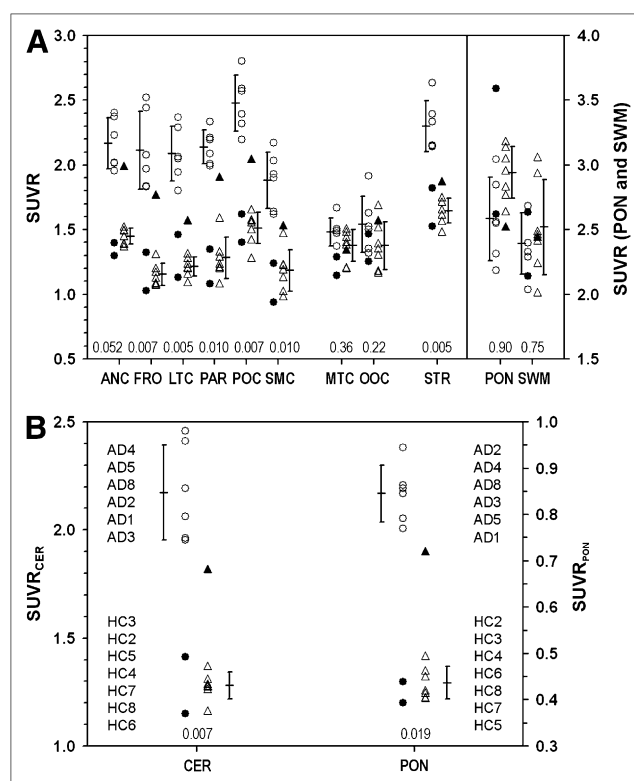


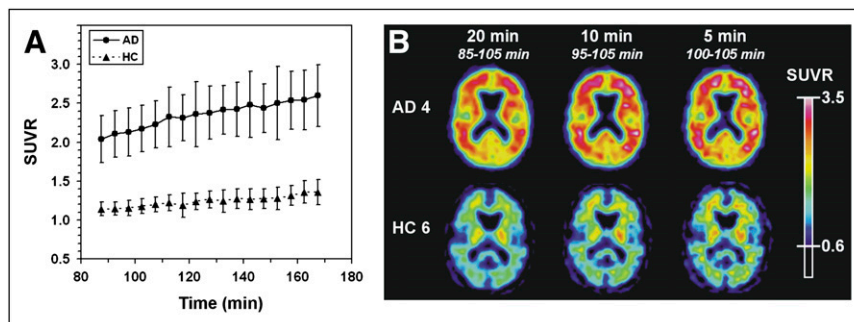
FIGURE 5. Pooled data for steps 1 and 2. (A) SUV ratios integrated over 85- to 105-min time window using cerebellum as reference region. (B) Composite cortical region: distribution of SUV ratios using cerebellum and pons as reference region for 85- to 105-min time window. Subject rank order within AD and control groups is given in left and right margins of respective dataset. Mean and SD for each group (excluding outliers) are represented with error bars. SUV ratios of pons and subcortical white matter are referred to a separate y-axis. *P* values (1-sided) denote significance of Wilcoxon/Mann-Whitney test to discriminate between entire AD group ($n = 8$) and healthy control group ($n = 8$). Circles = AD patients; triangles = healthy controls; filled symbols = outliers; ANC = anterior cingulate; CER = cerebellum; FRO = frontal cortex; LTC = lateral temporal cortex; MTC = medial temporal cortex; OOC = occipital cortex; PAR = parietal cortex; POC = posterior cingulate; PON = pons; SMC = sensorimotor cortex; STR = striatum; SUV = SUV ratio; SWM = subcortical white matter.

with the seven ^{18}F -flutemetamol-negative healthy controls using voxel-based statistics. Highly significant differences were found in neocortical association zones (Fig. 7).

DISCUSSION

We have shown that, when applied after 80 min, computationally simple methods using a reference region uptake ratio discriminate well between ^{18}F -flutemetamol-positive AD patients and ^{18}F -flutemetamol-negative healthy controls (Table 2; Figs. 4, 5, and 7), even for scanning times as short as 5–10 min (Fig. 6B). This discrimination was only marginally affected by the scanning start time (Fig. 6A) or

FIGURE 6. (A) Average SUV ratio curves (\pm SD) in frontal cortex over 85- to 170-min time window (5-min length) in AD patients (\bullet , $n = 6$) and healthy controls (\blacktriangle , $n = 7$). SUV ratios of outlier (Fig. 5) AD patients 6 and 7 and healthy control 1 were not included in this averaging. (B) Comparison of axial PET sum images of different scan lengths (5, 10, and 20 min) at constant scan end time (105 min) for 1 representative AD patient (AD patient 4) and 1 healthy control (healthy control 6). HC = healthy control; SUVr = SUV ratio.



scanning length (Fig. 6B) for time windows beyond 80 min. A recent analysis of different scanning windows for ^{11}C -PiB provides evidence that a 50- to 70-min scanning window is the overall best compromise for SUV ratio calculations (29). For the current ^{18}F agent, an acquisition window starting from 80 min onward appears to be most suitable.

The retention of ^{18}F -flutemetamol was similar in AD patients and healthy controls in brain regions known to be relatively unaffected by amyloid deposition, such as pons, cerebellum, and subcortical white matter (Table 2; Figs. 5 and 7). The exact quantification method used, DVR or SUV ratio, had little impact on the discriminatory power of ^{18}F -flutemetamol, in accordance with previous ^{11}C -PiB studies (30,31). Moreover, the choice of reference region, cerebellar cortex or pons, did not make much difference (Fig. 5B).

AD patients 6 and 7 showed an uptake pattern that was indistinguishable from the binding typical in healthy controls (Fig. 4, 5). Clinically and on neuropsychologic testing, these patients were comparable to the ^{18}F -flutemetamol-positive AD patients (Table 1). A small percentage (10%–20%) of patients with a diagnosis of clinically

probable AD who had received a ^{11}C -PiB PET scan in previous research studies also did not show elevated cortical tracer uptake (1,32,33). These negative scans may reflect limited sensitivity of the tracer (6,34) or, more likely, a lack of A β amyloid disease in these patients.

Conversely, healthy control 1 had increased ^{18}F -flutemetamol uptake. His values were at the lower end of those observed in AD. We cannot strictly rule out that increased cortical values partially resulted from spillover of white matter signal. However, the proportion of ^{18}F -flutemetamol-positive healthy controls in the current sample was comparable to the 10%–30% of cognitively intact elderly controls who show elevated ^{11}C -PiB brain uptake indistinguishable from AD (32,33,35–37).

The spatial distribution of ^{18}F -flutemetamol uptake in AD closely resembles that typically seen with ^{11}C -PiB binding (Fig. 7) (1,16,33,37–39). As in ^{11}C -PiB, striatal uptake of ^{18}F -flutemetamol was high and uptake in medial temporal cortex, one of the areas of predilection for neurofibrillary tangles in AD, relatively low. White matter uptake of ^{18}F -flutemetamol was conspicuous in a subset of healthy controls (e.g., healthy controls 3, 5, and 7 in Fig. 4). Statistically, this uptake did not differ between AD patients and healthy controls at the group level. White matter uptake probably reflects the slower clearance of the tracer from white matter than from the cortex (7).

Although reference region-based analysis methods (DVR and SUV ratio) performed well in discriminating AD patients from controls, the V_T values and kinetic rate constants from the input function-based kinetic modeling gave less consistent results. Similar to ^{11}C -PiB, the peripheral metabolism of ^{18}F -flutemetamol is rapid, and as a result the determination of intact tracer fractions at late time points suffers from high statistical variability (24). This can introduce a bias in the fitted intact fraction curve, which will in turn propagate into the results from input-based compartmental modeling. Use of the ratio of the distribution volumes in target and reference tissue, obtained from input function-based modeling, therefore appears a more robust approach, and the time-activity curve of an appropriate reference region can be used as an indirect input function to obtain ratios instead of absolute values. In

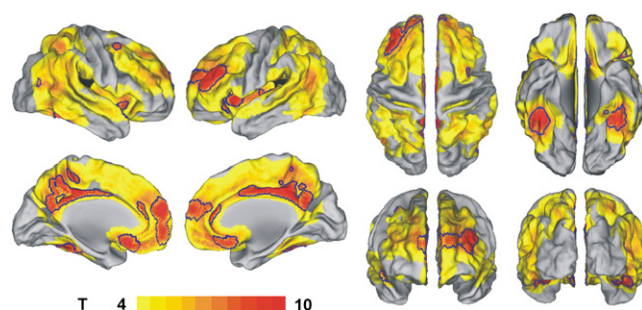


FIGURE 7. Surface rendering (CARET 5.51 (40)) of areas of significantly increased amyloid deposition in six ^{18}F -flutemetamol-positive AD patients compared with seven ^{18}F -flutemetamol-negative healthy controls, based on SUV ratio images integrated over 80–90 min (using cerebellum as reference region). Voxel-level uncorrected $P < 0.001$. Areas outlined in blue: voxel-level $P < 0.05$ corrected for whole brain volume.

our study, SUV ratio and DVR showed little variability and allowed good discrimination between AD patients and controls without the need for invasive and technically demanding blood sampling and analysis.

CONCLUSION

^{18}F -flutemetamol uptake can readily be quantified using reference region uptake ratios after 80 min and provides good discrimination between AD patients and healthy controls. These phase 1 results justify further pursuit of ^{18}F -flutemetamol as a biomarker for AD-related amyloidosis with wider availability for clinical and research purposes than its “parent molecule,” ^{11}C -PiB.

ACKNOWLEDGMENTS

We thank Carine Schildermans, Stijn Dirix, Hendrikje Jeandarme, Mieke Soons, and the Cyclotron Research Centre Liège, as well as the patients and healthy volunteers. This study was sponsored by GE Healthcare Ltd.

REFERENCES

1. Klunk WE, Engler H, Nordberg A, et al. Imaging brain amyloid in Alzheimer's disease with Pittsburgh compound-B. *Ann Neurol*. 2004;55:306–319.
2. Klunk WE, Wang Y, Huang GF, et al. The binding of 2-(4'-methylaminophenyl)benzothiazole to postmortem brain homogenates is dominated by the amyloid component. *J Neurosci*. 2003;23:2086–2092.
3. Klunk WE, Lopresti BJ, Ikonovic MD, et al. Binding of the positron emission tomography tracer Pittsburgh compound-B reflects the amount of amyloid-beta in Alzheimer's disease brain but not in transgenic mouse brain. *J Neurosci*. 2005;25:10598–10606.
4. Bacskai BJ, Frosch MP, Freeman SH, et al. Molecular imaging with Pittsburgh Compound B confirmed at autopsy: a case report. *Arch Neurol*. 2007;64:431–434.
5. Ikonovic MD, Klunk WE, Abrahamson EE, et al. Post-mortem correlates of in vivo PiB-PET amyloid imaging in a typical case of Alzheimer's disease. *Brain*. 2008;131:1630–1645.
6. Leinonen V, Alafuzoff I, Aalto S, et al. Assessment of beta-amyloid in a frontal cortical brain biopsy specimen and by positron emission tomography with carbon 11-labeled Pittsburgh compound B. *Arch Neurol*. 2008;65:1304–1309.
7. Fodero-Tavoletti MT, Rowe CC, McLean CA, et al. Characterization of PiB binding to white matter in Alzheimer disease and other dementias. *J Nucl Med*. 2009;50:198–204.
8. Bacskai BJ, Hickey GA, Skoch J, et al. Four-dimensional multiphoton imaging of brain entry, amyloid binding, and clearance of an amyloid-beta ligand in transgenic mice. *Proc Natl Acad Sci USA*. 2003;100:12462–12467.
9. Johnson KA, Gregas M, Becker JA, et al. Imaging of amyloid burden and distribution in cerebral amyloid angiopathy. *Ann Neurol*. 2007;62:229–234.
10. Lockhart A, Lamb JR, Osredkar T, et al. PiB is a non-specific imaging marker of amyloid-beta (Aβeta) peptide-related cerebral amyloidosis. *Brain*. 2007;130:2607–2615.
11. Greenberg SM, Grabowski T, Gurol ME, et al. Detection of isolated cerebrovascular beta-amyloid with Pittsburgh compound B. *Ann Neurol*. 2008;64:587–591.
12. Fodero-Tavoletti MT, Smith DP, McLean CA, et al. In vitro characterization of Pittsburgh compound-B binding to Lewy bodies. *J Neurosci*. 2007;27:10365–10371.
13. Klunk WE, Mathis CA. The future of amyloid-beta imaging: a tale of radionuclides and tracer proliferation. *Curr Opin Neurol*. 2008;21:683–687.
14. Koole M, Lewis DM, Buckley C, et al. Whole-body biodistribution and radiation dosimetry of ^{18}F -GE067: a radioligand for in vivo brain amyloid imaging. *J Nucl Med*. 2009;50:818–822.
15. Small GW, Kepe V, Ercoli LM, et al. PET of brain amyloid and tau in mild cognitive impairment. *N Engl J Med*. 2006;355:2652–2663.
16. Tolboom N, Yaqub M, van der Flier WM, et al. Detection of Alzheimer Pathology In Vivo Using Both ^{11}C -PiB and ^{18}F -FDDNP PET. *J Nucl Med*. 2009;50:191–197.
17. Rowe CC, Ackerman U, Browne W, et al. Imaging of amyloid beta in Alzheimer's disease with ^{18}F -BAY94-9172, a novel PET tracer: proof of mechanism. *Lancet Neurol*. 2008;7:129–135.
18. McKhann G, Drachman D, Folstein M, Katzman R, Price D, Stadlan EM. Clinical diagnosis of Alzheimer's disease: report of the NINCDS-ADRDA Work Group under the auspices of Department of Health and Human Services Task Force on Alzheimer's Disease. *Neurology*. 1984;34:939–944.
19. American Psychiatric Association. *Diagnostic and Statistical Manual of Mental Disorders*. 4th ed. Washington, DC: American Psychiatric Association; 1994.
20. Morris JC, Ernesto C, Schafer K, et al. Clinical dementia rating training and reliability in multicenter studies: the Alzheimer's Disease Cooperative Study experience. *Neurology*. 1997;48:1508–1510.
21. Anderson JL. A rapid and accurate method to realign PET scans utilizing image edge information. *J Nucl Med*. 1995;36:657–669.
22. Thurfjell L, Lau YH, Andersson JL, Hutton BF. Improved efficiency for MRI-SPET registration based on mutual information. *Eur J Nucl Med*. 2000;27:847–856.
23. Andersson JL, Thurfjell L. Implementation and validation of a fully automatic system for intra- and interindividual registration of PET brain scans. *J Comput Assist Tomogr*. 1997;21:136–144.
24. Price JC, Klunk WE, Lopresti BJ, et al. Kinetic modeling of amyloid binding in humans using PET imaging and Pittsburgh compound-B. *J Cereb Blood Flow Metab*. 2005;25:1528–1547.
25. Thal DR, Rüb U, Orantes M, Braak H. Phases of A beta-deposition in the human brain and its relevance for the development of AD. *Neurology*. 2002;58:1791–1800.
26. Lammertsma AA, Bench CJ, Price GW, et al. Measurement of cerebral monoamine oxidase B activity using L-[^{11}C]deprenyl and dynamic positron emission tomography. *J Cereb Blood Flow Metab*. 1991;11:545–556.
27. Syvänen S, Blomquist G, Appel L, Hammarlund-Udenaes M, Långström B, Bergström M. Predicting brain concentrations of drug using positron emission tomography and venous input: modeling of arterial-venous concentration differences. *Eur J Clin Pharmacol*. 2006;62:839–848.
28. Logan J, Fowler JS, Volkow ND, et al. Graphical analysis of reversible radioligand binding from time-activity measurements applied to [N- ^{11}C -methyl]-(-)-cocaine PET studies in human subjects. *J Cereb Blood Flow Metab*. 1990;10:740–747.
29. McNamee RL, Yee SH, Price JC, et al. Consideration of optimal time window for Pittsburgh compound B PET summed uptake measurements. *J Nucl Med*. 2009;50:348–355.
30. Lopresti BJ, Klunk WE, Mathis CA, et al. Simplified quantification of Pittsburgh Compound B amyloid imaging PET studies: a comparative analysis. *J Nucl Med*. 2005;46:1959–1972.
31. Yaqub M, Tolboom N, Boellaard R, et al. Simplified parametric methods for [^{11}C]PiB studies. *Neuroimage*. 2008;42:76–86.
32. Mintun MA, Larossa GN, Sheline YI, et al. [^{11}C]PiB in a nondemented population: potential antecedent marker of Alzheimer disease. *Neurology*. 2006;67:446–452.
33. Nelissen N, Vandenbulcke M, Fannes K, et al. Aβeta amyloid deposition in the language system and how the brain responds. *Brain*. 2007;130:2055–2069.
34. Klunk WE. Biopsy support for the validity of Pittsburgh compound B positron emission tomography with a twist. *Arch Neurol*. 2008;65:1281–1283.
35. Rowe CC, Ng S, Ackermann U, et al. Imaging beta-amyloid burden in aging and dementia. *Neurology*. 2007;68:1718–1725.
36. Aizenstein HJ, Nebes RD, Saxton JA, et al. Frequent amyloid deposition without significant cognitive impairment among the elderly. *Arch Neurol*. 2008;65:1509–1517.
37. Jack CR Jr, Lowe VJ, Senjem ML, et al. ^{11}C PiB and structural MRI provide complementary information in imaging of Alzheimer's disease and amnesic mild cognitive impairment. *Brain*. 2008;131:665–680.
38. Engler H, Forsberg A, Almkvist O, et al. Two-year follow-up of amyloid deposition in patients with Alzheimer's disease. *Brain*. 2006;129:2856–2866.
39. Edison P, Archer HA, Hinz R, et al. Amyloid, hypometabolism, and cognition in Alzheimer disease: an [^{11}C]PiB and [^{18}F]FDG PET study. *Neurology*. 2007;68:501–508.
40. Van Essen DC, Dickson J, Harwell J, Hanlon D, Anderson CH, Drury HA. An integrated software system for surface-based analyses of cerebral cortex. *JAMIA*. 2001;8:443–459.